Hydrol. Earth Syst. Sci. Discuss., 11, 9551–9588, 2014
www.hydrol-earth-syst-sci-discuss.net/11/9551/2014/
doi:10.5194/hessd-11-9551-2014

Hydrology and Earth System Sciences
Open Access
Discussions

Controls of macropore network characteristics on preferential solute transport

M. Larsbo, J. Koestel, and N. Jarvis

Department of Soil and Environment, Swedish University of Agricultural Sciences (SLU), P.O. Box 7014, 750 07 Uppsala, Sweden

Received: 4 July 2014 – Accepted: 21 July 2014 – Published: 12 August 2014

Correspondence to: M. Larsbo (mats.larsbo@slu.se)

Published by Copernicus Publications on behalf of the European Geosciences Union.

Abstract

In this study we examined the relationships between macropore network characteristics, hydraulic properties and state variables and measures of preferential transport in undisturbed columns sampled from four agricultural topsoils of contrasting texture and structure. Macropore network characteristics were computed from 3-dimensional X-ray tomography images of the soil pore system. Non-reactive solute transport experiments were carried out at five steady-state water flow rates from 2 to 12 mm h^{-1}. The degree of preferential transport was evaluated by the normalised 5 % solute arrival time and the apparent dispersivity calculated from the resulting breakthrough curves. Near-saturated hydraulic conductivities were measured on the same samples using a tension disk infiltrometer placed on top of the columns. Results showed that many of the macropore network characteristics were inter-correlated. For example, large macroporosities were associated with larger specific macropore surface areas and better local connectivity of the macropore network. Generally, an increased flow rate resulted in earlier solute breakthrough and a shifting of the peak concentration towards smaller drained volumes. Columns with smaller macroporosities, poorer local connectivity of the macropore network and smaller near-saturated hydraulic conductivities exhibited a greater degree of preferential transport. This can be explained by the fact that, with only two exceptions, global (i.e. sample-scale) continuity of the macropore network was still preserved at low macroporosities. Thus, for any given flow rate pores of larger diameter were actively conducting solute in soils of smaller near-saturated hydraulic conductivity. With less time for equilibration between the macropores and the surrounding matrix the transport became more preferential. Conversely, the large specific macropore surface area and well-connected macropore networks associated with columns with large macroporosities limit the degree of preferential transport because they increase the diffusive flux between macropores and the soil matrix and they increase the near-saturated hydraulic conductivity. The normalised 5 % arrival times were most strongly related with the estimated hydraulic state variables (e.g. with the degree of saturation

HESSD
11, 9551–9588, 2014

in the macropores $R^2 = 0.589$), since these combine into one measure the effects of irrigation rate and the near-saturated hydraulic conductivity function, which in turn implicitly depends on the volume, size distribution, global continuity, local connectivity and tortuosity of the macropore network.

1 Introduction

Preferential transport occurs when water containing solutes moves predominantly through a limited part of the soil pore space, bypassing the soil matrix. Preferential transport thus reduces the residence time for solutes in the unsaturated zone. The potential for preferential flow and transport is largely determined by soil properties with structured loamy and clayey soils generally having a large potential. In these soils, large inter-aggregate pores and biopores often act as pathways for fast transport of agrochemicals and contaminants (Thomas and Phillips, 1979).The extent to which the potential for preferential flow and transport is realized is determined by the initial and boundary conditions, where intense rainfall on initially wet soil generally leads to a high degree of preferential transport through any macropores open to the soil surface (Jarvis, 2007). Fast flow in macropores can even be generated when the soil is initially dry, especially if it has become water repellent (e.g. Jarvis et al., 2008).

The effects of flow rate on the transport of non-reactive solutes under steady-state water flow have been studied extensively using both controlled surface supply tensions (Seyfried and Rao, 1987; Langner et al., 1999; Yu et al., 2014) and controlled irrigation rates (Dyson and White, 1989; Haws et al., 2004; Pot et al., 2005). Generally the resulting solute breakthrough curves are shifted towards a smaller number of drained pore volumes and more skewed with higher flow rates and greater saturation indicating a higher degree of preferential transport. However, for some soils the water flow rate seems to have little or no effect on the shape of solute breakthrough curves (Dyson and White, 1989; Schulin et al., 1987). All of the above cited studies have used models to evaluate the degree of preferential transport. The most common approach has been

HESSD
11, 9551–9588, 2014

to fit both the convection-dispersion equation (CDE) and the mobile-immobile model (MIM) to the breakthrough curves. Equilibrium transport has been assumed if the fit of the CDE to the measured breakthrough curve is as good as the MIM. Optimized values for the parameters describing the immobile water content and the mass transfer rate between the mobile and immobile domains have been used as indicators of preferential transport (Langner et al., 1999). This approach is justified by the fact that the CDE is derived from assumptions of perfect lateral mixing (i.e. zero preferential transport). However, it has been shown that the CDE is very flexible and, hence, can be well fitted to breakthrough curves with a very fast breakthrough (Koestel et al., 2011). Deviations from the CDE may, therefore, not be a suitable indicator of preferential transport from a leaching risk perspective. Furthermore, the parameters in both the CDE and the MIM are often highly correlated which means that many parameter combinations may give equally good fits to measured data (Koch and Fluhler, 1993; Beven et al., 1993). Physical interpretations of fitted parameter values are, therefore, difficult. An attractive alternative to this approach is to evaluate the degree of preferential transport using model independent shape measures or indicators (Kamra and Lennartz, 2005; Koestel et al., 2011).

In many studies to date, indirect indicators of soil structure observed or measured at larger scales have been related to solute breakthrough curves (Vervoort et al., 1999; Jarvis, 2007) due to the lack of efficient experimental technologies to directly quantify structure at the pore scale. One method to quantify macropore networks is through analysis of 2-dimensional sections of resin-impregnated soil. However, this method is labour intensive and the number and size of investigated samples have, therefore, been limited. Holland et al. (2007) used this method to calculate pore network characteristics from two-dimensional images of horizontal soil sections and related these measures to breakthrough curves from non-reactive solute transport experiments carried out on separate columns. They fitted log-normal transit time distributions to the breakthrough curves and showed that breakthrough curves for columns with a less well connected pore network had smaller mean transit times and larger standard deviations

HESSD
11, 9551–9588, 2014

of transit times which we interpret as a higher degree of preferential transport. In recent years, non-destructive analysis of soil macropore networks has become possible through different 3-dimensional imaging techniques with X-ray tomography being the most common (Wildenschild and Sheppard, 2013). Quantitative measures of the macropore network (e.g. macroporosity, connectivity and tortuosity) can be calculated from X-ray tomography images. Although such measures are dependent on the original image quality, image processing methods and the algorithms used for calculating the measures they provide useful information on soil structure (Schlüter et al., 2014). Thus, X-ray tomography has the potential to link soil structural features to soil functioning. Although only a few studies have been reported, X-ray data has led to some new insights in the study of hydraulic and transport processes in soil. For example Vanderborght et al. (2002) used X-ray tomography to characterize the macropore network of a loamy forest soil. They showed that a dense macropore network at the 10–20 cm depth resulted in homogeneous transport whereas isolated large continuous macropores which were present at a depth of 50–60 cm resulted in more heterogeneous transport. Luo et al. (2010) showed that measures of macropore topology were correlated to saturated hydraulic conductivity and the dispersivities calculated from fitting the CDE to tracer breakthrough curves obtained under saturated conditions. They explained large dispersivity values, indicative of a high degree of preferential transport, with the presence of large continuous macropores. Kim et al. (2010) showed that measures of macropore topology could explain 79 % of the variation in saturated hydraulic conductivities. For many soils and climate conditions much of the transport takes place when the topsoil is not fully saturated. As far as we know, the relationships between macropore network characteristics derived from 3-dimensional images of the pore system and near-saturated hydraulic conductivity and solute transport during unsaturated flow have not yet been studied.

The objective of this study was to determine how macropore network characteristics influence near-saturated non-reactive tracer transport in agricultural topsoils. This was achieved by combining X-ray tomography with measurements of near-saturated

HESSD
11, 9551–9588, 2014

hydraulic conductivity using tension disk infiltrometers and non-reactive solute transport experiments carried out at different steady-state water flow rates in four soils of contrasting texture and structure.

2 Materials and methods

2.1 Soils

Soil columns were sampled in PVC pipes (20 cm high, 20 cm diameter) using a tractor mounted hydraulic press at four conventionally tilled fields close to Uppsala in eastern Sweden. Samples were taken from the topsoil leaving the soil surface undisturbed. The soils were Säby 1 (loam), Säby 2 (clay), Krusenberg (clay loam) and Ultuna (clay) (Table 1). These soils were chosen because they have clay contents above 20 % and, hence, were expected to have a well-developed structure (Horn et al., 1994) and a potential for preferential transport (Koestel and Jorda, 2014). The pore systems of cultivated topsoils change with time, for example due to tillage and subsequent consolidation and swelling/shrinking. In this study, all samples were taken on 26 June 2013. Three of the sampling sites (Säby 2, Krusenberg and Ultuna) were sown with spring crops a few weeks earlier (Table 1). At the time of sampling, the seedbeds for these soils consisted of fine individual aggregates. In contrast, dessication cracks extending a few cm down into the soil were visible for the Säby 1 soil which had been sown with an autumn crop. The samples were stored at 3 °C until the start of the solute breakthrough experiments. Since the natural soil surface was uneven, the length of the soil columns varied between 15.0–18.3 cm assuming that the soil surface was located where the soil matrix, as determined by X-ray tomography, filled at least 50 % of the horizontal column cross-section area.

One of the Säby 2 (clay) columns which contained a large amount of straw residues was accidentally destroyed during transport and one of the Ultuna (clay) columns ponded already at the lowest irrigation rate. These columns were excluded from the

HESSD
11, 9551–9588, 2014

study. Hence, transport experiments, X-ray tomography and measurements of near-saturated hydraulic conductivity were carried out on 18 out of the 20 columns (5 columns for Säby 1 (loam) and Krusenberg (clay loam) and 4 columns for Säby 1 (clay) and Ultuna (clay)).

2.2 Non-reactive solute transport experiments

Solute breakthrough experiments were conducted in an irrigation chamber at the Department of Soil and Environment at the Swedish University of Agricultural Sciences (SLU), during October and December 2013. The irrigation chamber is described in detail in Liu et al. (2012). Before the start of the experiments polyamide cloths (mesh size 50 µm) were attached to the bottom of the samples in order to minimize soil loss. The irrigation nozzles were turned on each minute and the flow rates were adjusted by setting the time each individual irrigation nozzle was on during one minute. To achieve the desired irrigation rates calibration was carried out before the start of each new irrigation. During the experiments the effluent water volumes were monitored daily. Irrigation intensities were not always constant at the nominal rates possibly due to the formation or dissolution of precipitates in the nozzles during the experiment. The actual average irrigation rates and their standard deviations estimated from effluent volumes are presented in Table S1 (Supplement).

The columns were first irrigated for 6 days with tap water at an intensity of 2 mm h^{-1} prior to the first solute application in order to allow the soil to settle and to achieve stable flow rates and background effluent electrical conductivities. Five tracer experiments were carried out under subsequently increasing steady-state irrigation rates of 2, 4, 6, 8 and 12 mm h^{-1}. As irrigation intensities increased the saturated hydraulic conductivities of a few columns were exceeded and surface ponding occurred. When a column ponded the transport was not further analysed. After an increase in irrigation rate a warm-up period was needed for the flow rates and background conductivities in the column effluents to stabilize. When the system was at approximate steady-state a 2 mL pulse of potassium bromide solution (250 mg bromide added per ml of tap water) was

HESSD
11, 9551–9588, 2014

applied during approximately 30 s at the surface of each column using a pipette. A reasonably homogeneous spatial application was achieved using a plastic grid placed on the surface before application. For all irrigation rates at least 185 mm water had passed through the columns when the experiments were stopped.

The electrical conductivity of the effluent was measured in flow-through vessels (D201, WTW GmbH, Weilheim, Germany) using electrical conductivity meters (Cond 3310, WTW GmbH, Weilheim, Germany). Measurements were recorded at 5 min resolution for the irrigation intensities 2–8 mm h^{-1} and at 1 min resolution for the 12 mm h^{-1} irrigation rate. Background electrical conductivities in the water supply were measured in grab samples taken approximately every 72 h throughout the experiment from one of the irrigation nozzles. The background electrical conductivities varied between 473 and 516 µS cm^{-1}. Furthermore, the background electrical conductivity of the effluent solution was influenced by resident ions in soil solution that reacted with the water flowing through the soil. We estimated the background concentration in the effluent solution during the experiments, $EC_{background}$, by fitting an equation of the form:

$$EC_{background}(t_i) = p_1 + p_2 t_i + p_3 \exp(p_4 t_i) \quad (1)$$

where p_1 to p_4 are fitted parameters, to the measured electrical conductivities during the time period prior to bromide application.

Bromide concentrations in the effluent water, C_{out} (mg mL^{-1}), were calculated from the electrical conductivity data assuming a linear relationship between bromide concentration and electrical conductivity:

$$C_{out}(t_i) = \frac{C_{in}(EC_{out}(t_i) - EC_{background}(t_i))}{(EC_{in} - EC_{background}(t_i))} \quad (2)$$

where C_{in} (mg mL^{-1}) is the known bromide concentration in the applied bromide solution, EC_{in} (µS cm^{-1}) and EC_{out} (µS cm^{-1}) are the electrical conductivities in the applied solution and in the effluent water respectively and t_i are the times when the electrical conductivity was recorded.

HESSD
11, 9551–9588, 2014

After the solute transport experiments the soil columns were left to drain for one week and then stored at 3 °C until the X-ray tomography was carried out.

2.3 Measures of preferential transport

Preferential transport is generally associated with an early arrival of solutes and pronounced tailing of solute breakthrough curves (Brusseau and Rao, 1990). In this study we used two shape measures to indicate the degree of preferential transport: the normalised 5 % arrival time which reflects the tendency for early arrival of the solutes and the Eulerean apparent dispersivity, hereafter referred to as the apparent dispersivity, which is a measure of the spread of arrival times (Knudby and Carrera, 2005; Koestel et al., 2011). The normalised 5 % arrival time has previously been shown to be strongly correlated to other model independent measures that reflect early solute arrival (Koestel et al., 2011; Ghafoor et al., 2013).

Traditionally solute breakthrough curves have been analysed in relation to the number of pore volumes that have passed through the sample. However, for unsaturated conditions the volumetric water content, θ (–), and, hence, the pore volume are usually unknown. We, therefore, used the solute breakthrough curve to define a "tracer-specific water filled pore volume" θ_{eff} as:

$$\theta_{\text{eff}} = \frac{q\mu_1}{L} \tag{3}$$

where q (mm h^{-1}) is the water flux per column cross-section area, L (mm) is the length of the soil column and μ_1 (h) is the normalised first temporal moment of the breakthrough curve (i.e. the average arrival time of the solute) given by:

$$\mu_1 = \frac{m_1}{m_0} = \frac{\int_0^\infty C_{\text{out}} t \mathrm{d}t}{\int_0^\infty C_{\text{out}} \mathrm{d}t} \tag{4}$$

where t (h) is time and m_0 (–) and m_1 (h) are the zeroth and first temporal moments, respectively. The integrals in Eq. (4) were estimated directly from the raw data.

HESSD
11, 9551–9588, 2014

A normalised breakthrough curve can be derived as (Jury and Roth, 1990):

$$g_n(T) = C_{\text{out}} \frac{\mu_1}{m_0} \tag{5}$$

where $T = t/\mu_1$ (–) is the number of effective pore volumes that has passed through the sample. The cumulative distribution function of the breakthrough curve is defined by:

$$G_n(T) = \int_0^T g_n \mathrm{d}T \tag{6}$$

The normalised 5 % arrival time, $p_{0.05}$, was finally calculated from:

$$G_n(p_{0.05}) = 0.05 \tag{7}$$

The 5 % arrival time is illustrated in Fig. 1. The apparent dispersivity which is a frequently used measure of the spread in solute arrival times (e.g. Vanderborght et al., 2001; Koestel et al., 2011) was calculated according to:

$$\lambda_{\text{app}} = \frac{\mu_2 L}{2\mu_1^2} \tag{8}$$

where L (cm) is the length of the soil column and μ_2 is the second central moment of the breakthrough curve given by:

$$\mu_2 = \int_0^\infty (t - \mu_1) \left(\frac{C_{\text{out}}}{m_0} \right) \mathrm{d}t \tag{9}$$

To enable a proper comparison between the breakthrough curves they were truncated at a time corresponding to 185 mm of applied water, which was the smallest amount that was applied in the experiments. Truncated breakthrough curves will generally result in overestimations of $p_{0.05}$ and underestimations of λ_{app} (Koestel et al., 2011).

HESSD
11, 9551–9588, 2014

2.4 X-ray computed tomography

In this study, we used the GE Phoenix v|tome|x m X-ray tomograph installed at the Department of Soil and Environment at SLU. It has a 240 kV X-ray tube, a tungsten target (beryllium window) and a GE 16″ flat panel detector. We collected 2000 radiographs per column with a discretization of 2024 pixels × 2024 pixels, corresponding to a resolution of 121.1 µm. The X-ray scans were carried out at a voltage of 200 kV with a current in the range 350–420 µA varying between columns. The exposure time for each radiograph was 250 µs. The radiographs were subsequently inverted to a 3-D image using the GE image reconstruction software datos|x and exported as TIFF-stacks (tagged image file format) with 16 bit greyscale resolution. The resulting spatial resolution of the reconstructed 3-D images was 121.1 µm in all directions. The X-ray tomography was carried out during December 2013 and February 2014, after the solute transport experiments.

2.5 Image processing and analysis

Image processing and analysis were carried out using the Fiji distribution (Schindelin et al., 2012) of the software ImageJ (Abramoff et al., 2004) including the plugin BoneJ (Doube et al., 2010), GeoDict (http://www.geodict.com) and R (R Core Team, 2012). First, the image resolution of each frame was reduced by a factor of two in all dimensions to limit the computation time during the following image processing steps. As a result, each image-voxel had an edge-length of 242.2 µm.

2.5.1 Definition of the sample volume

In order to calculate the soil macroporosity the total volume of the soil inside the PVC cylinder (hereafter referred to as the sample) needed to be estimated. Since the samples were taken from the soil surface their volumes were not identical. In order to define the sample volume, images were first rotated in order to get the columns in a perfectly

HESSD
11, 9551–9588, 2014

upright position. Then a circular region of interest corresponding to the inner diameter of the soil columns was defined and all image sections not containing soil were cut away. The 3-D image was imported into R as a sequence of vertical slices of the original image. The soil surface was determined by searching the first increase in grey value in each XY-coordinate that exceeded 25 % of the total range of grey values at that XY-coordinate, starting from the top of the soil column. All voxels above and below the soil surface were then set to 0 and 1, respectively. In order to fill surface vented pores with a radius smaller than approximately 2 mm we applied a two-dimensional mean filter using six neighbours to all zero valued voxels in each horizontal slice. The result of these operations was a binary image containing the sample volume.

2.5.2 Illumination correction and segmentation

The large column diameters and large soil bulk densities resulted in differences in illumination between the centre of the column and the perimeter. In addition, clear ring artefacts were visible at approximately 15 cm depth. These artefacts, caused by beam hardening, were reduced by first assigning all voxels in the sample volume into categories based on their vertical coordinate, z, and radial coordinate, r, (i.e. their distance from the centre of the column in the horizontal direction). All grey values, $GV_{x,y,z}$, were then corrected for radial differences in illumination according to:

$$GV_{corr,x,y,z} = Perc_{60,ref} + \frac{Perc_{80,ref} - Perc_{60,ref}}{Perc_{80,r,z} - Perc_{60,r,z}} \left(GV_{x,y,z} - Perc_{60,r,z}\right) \quad (10)$$

where $GV_{corr,x,y,z}$ are the corrected grey values, $Perc_{60,ref}$ and $Perc_{80,ref}$ are reference values for the 60th and 80th percentile grey values, respectively and $Perc_{60,r,z}$ and $Perc_{80,r,z}$ are the 60th and 80th percentiles of $GV_{x,y,z}$ at depth z and radial distance r. It was assumed that $Perc_{60,r,z}$ and $Perc_{80,r,z}$ represented the soil matrix and were, therefore, only marginally influenced by differences in macroporosity between categories (Iassanov and Tuller, 2010). Illumination corrections were done in R. The corrected images were filtered using the 3-D median filter with two neighbours in ImageJ

HESSD
11, 9551–9588, 2014

to reduce noise. A consequence of this filtering is the removal of the smallest pores. Finally, the images were binarized into macropores and soil matrix using Otsu's thresholding method (Otsu, 1979) applied to each slice. Hence, we defined macropores operationally as all pores visible in the binary images. Since the image resolution was 242.2 µm, pores with a diameter larger than approximately 484.4 µm were visible.

2.5.3 Measures of the macropore network

In addition to the total pore volume, a complete geometric and topological description of the pore network in soil should include metrics accounting for the size distribution of pores, their specific surface area and local connectivity (Vogel et al., 2010) as well as their heterogeneity and global (i.e. sample-scale) continuity (Renard and Allard, 2013). From the binary images of the pore networks we calculated a number of such measures of both the total macropore network and the largest macropore cluster connecting the soil surface to the bottom of the sample (Table 2). The total macropore network was divided into connected macropore clusters using the "Analyse particles" command in BoneJ. To estimate macropore sizes we calculated the pore "thickness" using BoneJ. The pore thickness is defined for each macropore voxel as the diameter of the largest sphere that fits into the macropore and contains the voxel. The histograms of thickness values were used as estimates of pore size distributions. Thicknesses were also calculated for the soil solid matrix as a proxy for aggregate size. The existence of a pore cluster connecting the soil surface to the bottom of the sample was used as an indicator of global continuity at the scale of the sample, while the Euler number for the largest connected cluster was used as an estimate of local pore connectivity (Vogel and Kretzschmar, 1996). The mass fractal dimension was calculated as a measure of the heterogeneity of the spatial distribution of macroporosity (Peyton et al., 1994; Perret et al., 2003). The smallest pore neck on the critical path connecting the soil surface to the bottom (the critical pore diameter) and the length of this path were estimated using the PoroDict module in GeoDict. The critical macropore diameter is estimated as

HESSD
11, 9551–9588, 2014

the diameter of the largest sphere that can pass through the pore space from the top to the bottom of the column.

2.6 Unsaturated hydraulic conductivity

After X-ray scanning, we measured the steady-state infiltration rate at the soil surface of each column with a tension disk infiltrometer set at supply tensions of $\psi = 5$ cm and $\psi = 1$ cm. The bottom plate of the tension infiltrometer had a diameter of 15 cm leaving space for air to escape through the soil surface near the column walls. A layer of moist fine sand was applied at the soil surface to ensure good contact between the tension disk and the soil. We used the steady-state infiltration rate as an estimate of the unsaturated hydraulic conductivity, K (mm h^{-1}), at the supply tension given the one-dimensional nature of the flow system.

The steady-state pressure potentials attained in the soil at the fluxes applied during the solute transport experiments were calculated assuming a linear relationship between $\log(\psi)$ and $\log(K)$ (Fig. 2) which is suggested by experimental observations (Jarvis et al., 2013). From the steady-state pressure potential we calculated the size of the largest water-filled pore during the solute transport experiments using the Young-Laplace capillarity equation. We then estimated the degree of saturation in the macropores at each flow rate from the X-ray derived pore size distribution.

2.7 Statistics

Spearman rank correlation coefficients were calculated between macropore characteristics, hydraulic conductivities and measures of preferential transport. Selected correlations were also graphically displayed and analysed by linear regression. For both cases results were considered significant if p values < 0.05.

HESSD
11, 9551–9588, 2014

3 Results and discussion

3.1 Soil characteristics

Figure 3 shows example images of the macropore networks generated by X-ray tomography for the four soils. All soils had larger macroporosities in the top 5 cm which corresponds to the harrowed layer. Macroporosities estimated from X-ray tomography images were between 3.3 and 12 % (Fig. 4) with an average value of 6.5 %. These values are large compared to macroporosities derived from X-ray tomography images reported in the literature for agricultural topsoils (Kim et al., 2010; Luo et al., 2010; Naveed et al., 2013). It should be noted that three of the soils included in this study were sampled a few weeks after ploughing and seedbed preparation, operations which generally increase macroporosity. Near saturated hydraulic conductivities at the pressure potentials of −1 and −5 cm, K_1 and K_5, were in the ranges 0.35 to 38 mm h^{-1} and 0.14 to 0.72 mm h^{-1}, respectively (Fig. 4), which is in line with previously reported values for loamy and clayey agricultural topsoils (Jarvis et al., 2013).

Macropore network characteristics are presented in Tables S2 and S3 in the Supplement. Figure 5 shows that many of the macropore network characteristics were inter-correlated. Here we briefly discuss the implications of some of these correlations. The positive correlation between macroporosity and fractal dimension shows that the macropore networks in columns with large macroporosities are spatially more homogeneously arranged (i.e. they "fill" the total volume to a larger extent). This space-filling property of columns with large macroporosities is also indicated by the strong negative correlation between macroporosity and mean aggregate width. Dal Ferro et al. (2013) reported positive correlations between macroporosity and fractal dimension for a silty to sandy loam soil under different fertilization regimes. Positive correlations have also been reported between depth distributions of macroporosity and fractal dimension for a sandy loam soil (Perret et al., 2003) and a silty loam soil (Luo and Lin, 2009).

HESSD
11, 9551–9588, 2014

A positive correlation was found between macroporosity and the fraction of the total pore space consisting of the largest pore cluster. As might be expected, the Euler number, as a measure of local connectivity, showed a significant negative correlation with the macroporosity of the largest pore cluster and the fraction of the total macroporosity which was found in this cluster, although the negative correlation between the Euler number and total macroporosity was not significant. These results indicate that large macroporosities are associated with a more connected macropore network. This relationship is also suggested by the global connectivity measure, C, which indicates whether any pore cluster extends from the top to the bottom of the column ($C = 1$) or not ($C = 0$). The two columns where such a cluster did not exist had the second and third smallest macroporosities out of the 18 columns (Table S2, Supplement). Figure 5 also shows that samples with larger total macroporosity and better connected macropore networks (i.e. with a smaller Euler number) had significantly larger hydraulic conductivities at 1 cm tension.

3.2 Solute transport

Figure 6 shows that, as reported in previous studies (Koestel et al., 2012; Ghafoor et al., 2013), the two measures describing the shape of the breakthrough curve, the normalised 5 % arrival time and the apparent dispersivity, were strongly correlated to each other, especially for columns exhibiting only weak preferential transport. Therefore, in the following we mainly discuss the normalised 5 % arrival times, which generally showed slightly stronger correlations with the macropore network characteristics, state variables and hydraulic properties of the soils.

All solute breakthrough curves are presented in Figs. S1 to S4 in the Supplement. Generally, an increased flow rate resulted in earlier breakthrough and a shifting of the peak concentration towards smaller drained volumes which is in line with previous studies (e.g. Haws et al., 2004; Pot et al., 2005; Koestel et al., 2012). The relationship between peak height and the flow rate was less clear (Fig. S1 to S4 in the Supplement).

HESSD
11, 9551–9588, 2014

Although peak heights may contain interesting information regarding the transport process they were not further considered in this study.

The normalised 5 % arrival times and apparent dispersivities are presented in Table S4 in the Supplement. Forty-three percent of the breakthrough curves had normalised 5 % arrival times smaller than the median value of approximately 0.25 for 302 breakthrough curves from undisturbed soil columns sampled from arable land, which are included in the meta-analysis of Koestel et al. (2012) while 39 % had apparent dispersivities larger than the median value of approximately 10 cm for the same data set. Figure 7 shows that the normalised 5 % arrival times varied between 0.04 and 0.50 for the four soils. The decreasing number of data points with increasing flow rate for Säby 1 (loam), Säby 2 (clay) and Ultuna (clay) is due to surface ponding. The pattern seen in Fig. S1 to S4 with decreasing normalised 5 % arrival times at higher flow rates was not apparent in the average values for the two clay soils. This is because the columns that ponded had smaller normalised 5 % arrival times than the average values. Figure 7 shows that it is not possible to make a general statement comparing the degree of preferential transport in different soils based on breakthrough curves from one flow rate only. For example at an irrigation rate of 2 mm h^{-1} Säby 2 (clay) exhibits stronger preferential transport than Säby 1 (loam), although this is not statistically significant, while the opposite is true for irrigation rates higher than 4 mm h^{-1}.

3.2.1 Relationships between macropore network characteristics and measures of preferential transport

Figure 8 shows the relationships between pore network characteristics and measures of preferential transport. Significant positive correlations were found between the normalised 5 % arrival times and macroporosity at irrigation rates between 2 and 6 mm h^{-1} (Fig. 8a). These results indicate that preferential solute transport was significantly weaker in the columns with large macroporosities, which also contained more homogeneously distributed and better-connected macropore networks and had larger hydraulic conductivities close to saturation (Fig. 5). At first sight, these results may seem counter-

HESSD
11, 9551–9588, 2014

intuitive. However, this relationship can be explained by the fact that macropores will fill up until the hydraulic conductivity of the soil is large enough to conduct water at the set flow rate. For soils with small macroporosities a larger fraction of the macroporosity must be water filled (i.e. the degree of saturation in the macropores is larger) at the given flow rate (assuming similar pore size distributions). This means that pores with larger diameter, which conduct water at higher flow rates, will be active in the transport. With less time for equilibration of solute concentrations between the macropores and the surrounding matrix the transport becomes more preferential. The important role of diffusion in controlling preferential transport in macroporous soils has previously been discussed in a number of studies (e.g. Jarvis et al., 1991; Gerke and van Genuchten, 1993; Koestel and Larsbo, 2014). In our study, normalised 5 % arrival times were positively correlated to the specific macropore surface area and negatively correlated to mean aggregate thickness (Figs. 5 and 8c). These two macropore network characteristics were in turn negatively correlated to each other. For an ideal aggregate geometry (e.g. uniform sized cubes or spheres), they would be perfectly correlated. These results suggest that a larger area for diffusive exchange between macropores and the soil matrix increases the diffusive flux, thereby limiting preferential transport. The significance of aggregate thickness may also partly reflect the effects of pore connectivity on preferential transport, since soils with smaller aggregates also have a denser and better connected macropore network compared to soils with larger aggregates (Fig. 5).

The Euler number was negatively correlated to the normalised 5 % arrival times, although only significantly for the two lowest irrigation rates (Fig. 8g). This means that pore clusters that are locally more connected (i.e. smaller Euler number) are associated with a lower degree of preferential transport. It seems that providing global continuity is maintained, which was the case for all but two columns in this study, a less connected pore network leads to stronger preferential transport. These results support the conceptual model described by Jarvis (2007) and further elaborated on by Jarvis et al. (2012), where the strongest preferential transport was predicted to occur in soils with large continuous macropores with poorly connected networks of smaller

HESSD
11, 9551–9588, 2014

macropores and mesopores. A well-connected network of smaller pores reduces the likelihood of soil water potentials increasing sufficiently to trigger flow in the largest macropores and increase rates of lateral convective and diffusive mass exchange during vertical flow. At first glance, these findings may seem to contradict the results of numerical studies carried out at the macroscopic Darcy-scale, where better connected flow pathways (zones of high hydraulic conductivity correlated in the direction of flow) have been shown to promote preferential transport (e.g. Knudby and Carrera, 2005; Bianchi et al., 2011). However, there is no conflict between these findings at the pore and Darcy scales. This is illustrated schematically in Fig. 9, which shows that providing pore continuity across the sample is maintained, decreased macroporosity and associated poor local connectivity at the pore scale should result in stronger preferential transport. At the macroscopic Darcy-scale this will be manifested as spatially correlated high conductivity flow pathways surrounded by low conductivity zones.

To our knowledge, only two previous studies have investigated the relationships between imaged macropore network characteristics and preferential solute transport. Similar to our results, Luo et al. (2010) found that soil columns with larger macroporosities showed slower solute breakthrough. The node density, which they used as a measure of local connectivity, was also positively correlated to macroporosity. Holland et al. (2007) showed that breakthrough curves for columns with a less well connected pore network had smaller mean transit times and larger standard deviations of transit times. These columns also had smaller macroporosities and specific macropore surface areas.

The correlations between pore network characteristics and measures of preferential transport were generally stronger at the lower irrigation rates (Figs. 5 and 8). One reason for this is simply that there were fewer columns for the higher irrigation rates due to surface ponding. Another tentative explanation is that the calculated pore network characteristics depend mostly on the smaller macropores that dominate transport at lower flow rates. For example the Euler number is mainly determined by the dense network of finer pores while the transport at higher irrigation rates is to a larger extent

HESSD
11, 9551–9588, 2014

determined by the larger macropores which comprise a smaller fraction of the total imaged pore volume.

3.2.2 Relationships between hydraulic properties and state variables and measures of preferential transport

Figure 10 shows the relationships between hydraulic properties and state variables and measures of preferential transport. The positive correlation between near-saturated hydraulic conductivity and 5 % arrival times was significant for all irrigation rates (Fig. 10a). This shows that columns with high near-saturated conductivities exhibit a low degree of preferential transport. This was also found by Ghafoor et al. (2013) for a large dataset of 45 topsoil columns sampled from 14 agricultural fields in a small catchment in south-east Sweden. Again, this relationship arises because at any given applied irrigation rate, larger pores will become water-filled in soils of lower near-saturated hydraulic conductivity. This will tend to enhance the degree of preferential transport providing macropore continuity does not break down at the sample scale. This is further illustrated by Fig. 10c and d, which shows a strong relationship between the degree of preferential transport and the estimated size of the largest water-filled macropore (R^2 = 0.485 and 0.438 for all data in Fig. 10c and d, respectively). A similar relationship was previously reported by Ghafoor et al. (2013). Since the near-saturated hydraulic conductivity is dependent on the pore volume as well as the continuity, connectivity and tortuosity of the macropore network these properties are implicitly accounted for in the calculations of the largest water-filled pores. Plotting the data in this way greatly reduces the scatter due to variations in irrigation rate, which is apparent in the plots of breakthrough shape measures against pore network characteristics (Fig. 8) and hydraulic conductivity (Fig. 10a and b). This is even more apparent in the relationships between the degree of saturation and the normalised 5 % arrival times and apparent dispersivity shown in Fig. 10e and f (R^2 = 0.589 and 0.520 for all data in Fig. 10e and f, respectively). In addition to the diameter of the largest water-filled macropores, it is reasonable to assume that the fraction of macropores with a diameter close to the

HESSD
11, 9551–9588, 2014

diameter of the largest water-filled pore in relation to the total water-filled macropore volume (i.e. the pore size distribution of the water-filled macropores) should affect the degree of preferential transport. A strong correlation between the degree of saturation and normalised 5 % solute arrival times was also found by Koestel et al. (2013) for 65 topsoil columns sampled from one agricultural field in Denmark.

There are many possible reasons for the remaining unexplained scatter in the data. Most importantly the transport behaviour of these soils should not be expected to be fully determined by the degree of saturation. As discussed above the specific macropore surface area will affect the degree of preferential transport through its influence on the diffusive exchange between pore domains (Fig. 8c and d). Characteristics of the pores with sizes below the resolution of the images are also likely to influence solute transport. The estimated largest water-filled pores and, hence, the degree of saturation is dependent on the validity of the assumption of a linear relationship between $\log(\psi)$ and $\log(K)$. The calculated macropore characteristics are estimates of the true soil properties whose accuracy depends on the quality of the images and the image processing procedure. The estimated normalised 5 % arrival times and apparent dispersivities are dependent on the accuracy of the subtraction of background electrical conductivity values and were possibly also influenced by fluctuations in the irrigation rate (Table S1 in the Supplement). Finally, it can be noted that the macropore networks are not constant with depth (Fig. 3) and the use of averages for the whole sample may, therefore, not be appropriate. Considering all these uncertainties and potential sources of error we consider that the relationships shown in Figs. 8 and 10 are remarkably strong.

4 Conclusions

The results of this study indicate that soils with large macroporosities are associated with a well-connected, space-filling macropore network with a large specific macropore surface area. These properties limit the degree of preferential transport because

HESSD
11, 9551–9588, 2014

they increase the diffusive flux between macropores and the soil matrix and increase the near-saturated hydraulic conductivity, thereby inactivating the largest pores during solute transport under steady near-saturated flow. Our results suggest that the near-saturated hydraulic conductivity potentially could be used as a predictor of preferential transport. This is because the near-saturated hydraulic conductivity function implicitly contains information on key aspects of macropore geometry and topology, including size distributions, tortuosities, local connectivity and global continuity.

This study was carried out on conventionally-tilled agricultural topsoils with clay contents above 20 % using constant irrigation intensities from 2 to 12 mm h^{-1} which resulted in nearly saturated conditions. The extent to which the conclusions of our study with respect to the relationships between pore network characteristics and flow and transport properties can be extrapolated to other soil and climatic conditions should be the subject of further research. However, it is encouraging that our results are in agreement with the general conceptual model proposed by Jarvis et al. (2012) and are also supported by the results of the only two previous studies we are aware of that have investigated these relationships (Holland et al., 2007; Luo et al., 2010).

The Supplement related to this article is available online at doi:10.5194/hessd-11-9551-2014-supplement.

Acknowledgements. This study was funded by the Royal Swedish Academy of Agriculture and Forestry and the Centre for Chemical Pesticides (SLU). We thank Julien Moeys at the Department of Soil and Environment (SLU) for improving the R scripts used for image analysis.

References

Abramoff, D., Magalhaes, P. J., and Ram, S. J.: Image processing with ImageJ, Biophotonics Int., 11, 36–42, 2004.

HESSD
11, 9551–9588, 2014

Beven, K. J., Henderson, D. E., and Reeves, A. D.: Dispersion parameters for undisturbed partially saturated soil, J. Hydrol., 143, 19–43, 1993.
Bianchi, M., Zheng, C., Wilson, C., Tick, G. R., Liu, G., and Gorelick, S. M.: Spatial connectivity in a highly heterogeneous aquifer: from cores to preferential flow paths, Water Resour. Res., 47, W05524, doi:10.1029/2009WR008966, 2011.
Brusseau, M. L. and Rao, P. S. C.: Modeling solute transport in structured soils – a review, Geoderma, 46, 169–192, 1990.
Dal Ferro, N., Charrier, P., and Morari, F.: Dual-scale micro-CT assessment of soil structure in a long-term fertilization experiment, Geoderma, 204, 84–93, 2013.
Doube, M., Klosowski, M. M., Arganda-Carreras, I., Cordelieres, F. P., Dougherty, R. P., Jackson, J. S., Schmid, B., Hutchinson, J. R., and Shefelbine, S. J.: BoneJ Free and extensible bone image analysis in ImageJ, Bone, 47, 1076–1079, 2010.
Dyson, J. S. and White, R. E.: The effect of irrigation rate on solute transport in soil during steady water flow, J. Hydrol., 107, 19–29, 1989.
Gerke, H. H. and van Genuchten, M. T.: A dual-porosity model for simulating the preferential movement of water and solutes in structured porous media, Water Resour. Res., 29, 305–319, 1993.
Ghafoor, A., Koestel, J., Larsbo, M., Moeys, J., and Jarvis, N.: Soil properties and susceptibility to preferential solute transport in tilled topsoil at the catchment scale, J. Hydrol., 492, 190–199, 2013.
Haws, N. W., Das, B. S., and Rao, P. S. C.: Dual-domain solute transfer and transport processes: evaluation in batch and transport experiments, J. Contam. Hydrol., 75, 257–280, 2004.
Holland, J. E., White, R. E., and Edis, R.: The relation between soil structure and solute transport under raised bed cropping and conventional cultivation in south-western Victoria, Austral, J. Soil Res., 45, 577–585, 2007.
Horn, R., Taubner, H., Wuttke, M., and Baumgartl, T.: Soil physical properties related to soil structure, Soil Till. Res., 30, 187–216, 1994.
Iassonov, P. and Tuller, M.: Application of segmentation for correction of intensity bias in X-ray computed tomography images, Vadose Zone J., 9, 187–191, 2010.
Jarvis, N. J.: A review of non-equilibrium water flow and solute transport in soil macropores: principles, controlling factors and consequences for water quality, Eur. J. Soil Sci., 58, 523–546, 2007.

HESSD
11, 9551–9588, 2014

Jarvis, N. J., Bergström, L., and Dik, P. E.: Modelling water and solute transport in macroporous soil, II. Chloride breakthrough under non-steady flow, J. Soil Sci., 42, 71–81, 1991.
Jarvis, N. J., Etana, A., and Stagnitti, F.: Water repellency, near-saturated infiltration and preferential solute transport in a macroporous clay soil, Geoderma, 143, 223–230, 2008.
Jarvis, N. J., Moeys, J., Koestel, J., and Hollis, J. M.: Preferential flow in a pedological perspective, in: Hydropedology: Synergistic Integration of Soil Science and Hydrology, edited by: Lin, H., Academic Press, Elsevier B.V., Amsterdam, 75–120, 2012.
Jarvis, N., Koestel, J., Messing, I., Moeys, J., and Lindahl, A.: Influence of soil, land use and climatic factors on the hydraulic conductivity of soil, Hydrol. Earth Syst. Sci., 17, 5185–5195, doi:10.5194/hess-17-5185-2013, 2013.
Jury, W. A. and Roth, K.: Transfer Functions and Solute Movement Through Soil: Theory and Applications, Birkhauser Verlag AG, Basel Switzerland, 226 pp., 1990.
Kamra, S. K. and Lennartz, B.: Quantitative indices to characterize the extent of preferential flow in soils, Environ. Modell. Softw., 20, 903–915, 2005.
Kim, H., Anderson, S. H., Motavalli, P. P., and Gantzer, C. J.: Compaction effects on soil macropore geometry and related parameters for an arable field, Geoderma, 160, 244–251, 2010.
Knudby, C. and Carrera, J.: On the relationship between indicators of geostatistical, flow and transport connectivity, Adv. Water Resour., 28, 405–421, 2005.
Koch, S. and Fluhler, H.: Solute transport in aggregated porous media: comparing model independent and dependent parameter estimation, Water Air Soil Poll., 68, 275–289, 1993.
Koestel, J. and Jorda, H.: What determines the strength of preferential transport in undisturbed soil under steady-state flow?, Geoderma, 217, 144–160, 2014.
Koestel, J. and Larsbo, M.: Imaging and quantification of preferential solute transport in soil macropores, Water Resour. Res., 50, 4357–4378, 2014.
Koestel, J. K., Moeys, J., and Jarvis, N. J.: Evaluation of nonparametric shape measures for solute breakthrough curves, Vadose Zone J., 10, 1261–1275, 2011.
Koestel, J. K., Moeys, J., and Jarvis, N. J.: Meta-analysis of the effects of soil properties, site factors and experimental conditions on solute transport, Hydrol. Earth Syst. Sci., 16, 1647–1665, doi:10.5194/hess-16-1647-2012, 2012.
Koestel, J. K., Norgaard, T., Luong, N. M., Vendelboe, A. L., Moldrup, P., Jarvis, N. J., Lamande, M., Iversen, B. V., and de Jonge, L. W.: Links between soil properties and steady-state solute transport through cultivated topsoil at the field scale, Water Resour. Res., 49, 790–807, 2013.

HESSD
11, 9551–9588, 2014

Langner, H. W., Gaber, H. M., Wraith, J. M., Huwe, B., and Inskeep, W. P.: Preferential flow through intact soil cores: Effects of matric head, Soil Sci. Soc. Am. J., 63, 1591–1598, 1999.
Larsbo, M., Stenström, J., Etana, A., Börjesson, E., and Jarvis, N. J.: Herbicide sorption, degradation, and leaching in three Swedish soils under long-term conventional and reduced tillage, Soil Till. Res., 105, 200–208, 2009.
Liu, J., Aronsson, H., Ulén, B., and Bergström, L.: Potential phosphorus leaching from sandy topsoils with different fertilizer histories before and after application of pig slurry, Soil Use Manage., 28, 457–467, 2012.
Luo, L. and Lin, H.: Lacunarity and fractal analyses of soil macropores and preferential transport using micro-X-ray computed tomography, Vadose Zone J., 8, 233–241, 2009.
Luo, L., Lin, H., and Schmidt, J.: Quantitative relationships between soil macropore characteristics and preferential flow and transport, Soil Sci. Soc. Am. J., 74, 1929–1937, 2010.
Naveed, M., Moldrup, P., Arthur, E., Wildenschild, D., Eden, M., Lamandé, M., Vogel, H.-J., and de Jonge, L. W.: Revealing soil structure and functional macroporosity along a clay gradient using X-ray computed tomography, Soil Sci. Soc. Am. J., 77, 403–411, 2013.
Otsu, N.: Threshold selection method from grey-level histograms, IEEE T. Syst. Man Cyb., 9, 62–66, 1979.
Perret, J. S., Prasher, S. O., and Kacimov, A. R.: Mass fractal dimension of soil macropores using computed tomography: from the box-counting to the cube-counting algorithm, Eur. J. Soil Sci., 54, 569–579, 2003.
Peyton, R. L., Gantzer, C. J., Anderson, S. H., Haeffner, B. A., and Pfeifer, P.: Fractal dimension to describe soil macropore structure using X-ray computed tomography, Water Resour. Res., 30, 691–700, 1994.
Pot, V., Simunek, J., Benoit, P., Coquet, Y., Yra, A., and Martinez-Cordon, M. J.: Impact of rainfall intensity on the transport of two herbicides in undisturbed grassed filter strip soil cores, J. Contam. Hydrol., 81, 63–88, 2005.
R Core Team: R: a Language and Environment for Statistical Computing, R Foundation for Statistical Computing, Vienna, Austria, ISBN 3-900051-07-0, available at: http://www.R-project.org/ (last access: 1 July 2014), 2012.
Renard, P. and Allard, D.: Connectivity metrics for subsurface flow and transport, Adv. Water Resour., 51, 168–196, 2013.
Seyfried, M. S. and Rao, P. S. C.: Solute transport in undisturbed columns of an aggregated tropical soil: preferential flow effects, Soil Sci. Soc. Am. J., 51, 1434–1444, 1987.

HESSD
11, 9551–9588, 2014

Schindelin, J., Arganda-Carreras, I., Frise, E., Kaynig, V., Longair, M., Pietzsch, T., Preibisch, S., Rueden, C., Saalfeld, S., Schmid, B., Tinevez, J.-Y., White, D. J., Hartenstein, V., Eliceiri, K., Tomancak, P., and Cardona, A.: Fiji: an open-source platform for biological-image analysis, Nat. Methods, 9, 676–682, 2012.

Schlüter, S., Sheppard, A., Brown, K., and Wildenschild, D.: Image processing of multiphase images obtained via X-ray microtomography: a review, Water Resour. Res., 50, 3615–3639, 2014.

Schulin, R., Wierenga, P. J., Fluhler, H., and Leuenberger, J.: Solute transport through a stony soil, Soil Sci. Soc. Am. J., 51, 36–42, 1987.

Thomas, G. W. and Phillips, R. E.: Consequences of water-movement in macropores, J. Environ. Qual., 8, 149–152, 1979.

Vanderborght, J., Vanclooster, M., Timmerman, A., Seuntjens, P., Mallants, D., Kim, D. J., Jacques, D., Hubrechts, L., Gonzalez, C., Feyen, J., Diels, J., and Deckers, J.: Overview of inert tracer experiments in key Belgian soil types: relation between transport and soil morphological and hydraulic properties, Water Resour. Res., 37, 2873–2888, 2001.

Vanderborght, J., Gahwiller, P., and Fluhler, H.: Identification of transport processes in soil cores using fluorescent tracers, Soil Sci. Soc. Am. J., 66, 774–787, 2002.

Vervoort, R. W., Radcliffe, D. E., and West L. T.: Soil structure development and preferential solute flow, Water Resour. Res., 35, 913–928, 1999.

Vogel, H.-J. and Kretzschmar, A.: Topological characterization of pore space in soil – sample preparation and digital image-processing, Geoderma, 73, 23–38, 1996.

Vogel, H.-J., Weller, U., and Schlüter, S.: Quantification of soil structure based on Minkowski functions, Comput. Geosci., 36, 1236–1245, 2010.

Wildenschild, D. and Sheppard, A. P.:, X-ray imaging and analysis techniques for quantifying pore-scale structure and processes in subsurface porous medium systems, Adv. Water Resour., 51, 217–246, 2013.

Yu, Z. B., Dong, W. Q., Young, M. H., Li, Y. P., and Yang. T.: On evaluating characteristics of the solute transport in the arid vadose zone, Ground Water, 52, 50–62, 2014.

HESSD
11, 9551–9588, 2014

Table 1. Soil properties.

Site	Soil type	Clay (%)	Silt (%)	Sand (%)	Total organic carbon content ($g\,kg^{-1}$)	Crop 2013
Säby 1[1]	loam	21.0	47.3	31.7	19.7	Autumn sown wheat
Säby 2	clay	46.8	33.0	20.2	24.5[2]	Spring sown barley
Ultuna[1]	clay	45.8	39.2	15.0	27.5	Spring sown peas
Krusenberg	clay loam	32.3	33.1	34.6	13.0	Spring sown barley

[1] Data from Larsbo et al. (2009).
[2] Estimated as 50 % of the mass lost on ignition.

HESSD
11, 9551–9588, 2014

Table 2. Measures of the macropore network.

Measure	Unit	Description
Total macropore system		
Macroporosity	–	Volume of macropores/total sample volume
Specific macropore surface area	$mm^2\ mm^{-3}$	Surface area of macropores/total sample volume
Hydraulic radius	mm	Macropore volume/surface area
Mean pore thickness	mm	Mean value of thicknesses of the macropore network
Mean aggregate thickness	mm	Mean value of thicknesses of the soil matrix
Fractal dimension	–	Mass fractal dimension of the macropore network
Global connectivity	–	Existence of a pore cluster connecting the soil surface to the bottom (1 if cluster exists, 0 otherwise)
Largest connected cluster		
Fraction of macropore volume	–	Fraction of total macropore volume occupied by the largest connected cluster
Mean pore thickness	mm	Mean value of thicknesses of the largest connected cluster
Euler number	–	A measure of local connectivity
Critical pore diameter	mm	The smallest diameter of the largest connected macropore
Tortuosity	–	Path length (i.e. the shortest path from the surface to the bottom with pore diameters larger than or equal to the critical pore diameter) divided by the length of the sample

HESSD
11, 9551–9588, 2014

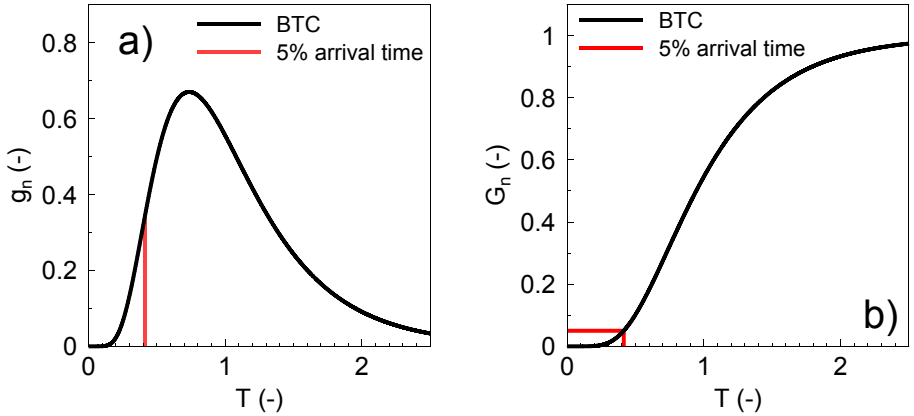

Figure 1. Illustration of the normalised 5 % arrival time, $p_{0.05}$. **(a)** shows the travel-time probability density function, g_n, where the area to the left of the 5 % arrival time equals 5 % of the total area under the curve and **(b)** shows the corresponding cumulative distribution function of the travel times, G_n. Both curves are plotted against the number of effective pore volumes drained (T).

HESSD
11, 9551–9588, 2014

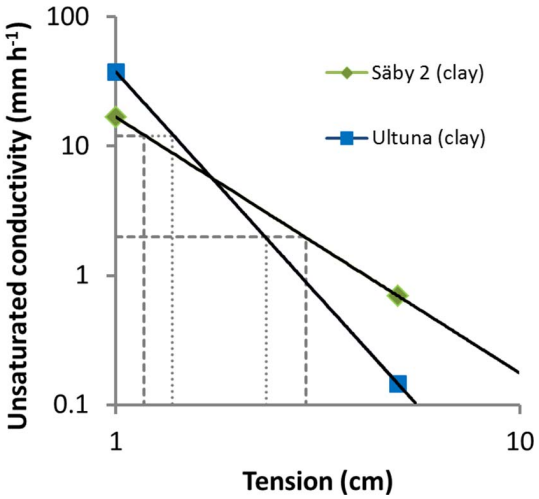

Figure 2. Illustration of soil tensions corresponding to irrigation rates 2 and 12 mm h^{-1} for two of the columns.

HESSD
11, 9551–9588, 2014

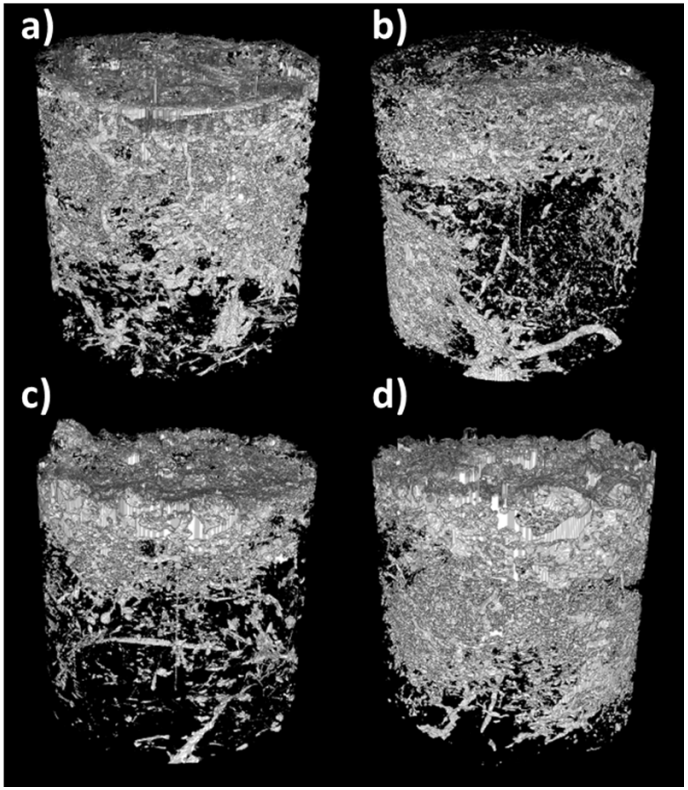

Figure 3. Examples of 3-D reconstructions of the visible pore space **(a)** Säby 1 (loam), **(b)** Säby 2 (clay), **(c)** Ultuna (clay) and **(d)** Krusenberg (clay loam).

HESSD
11, 9551–9588, 2014

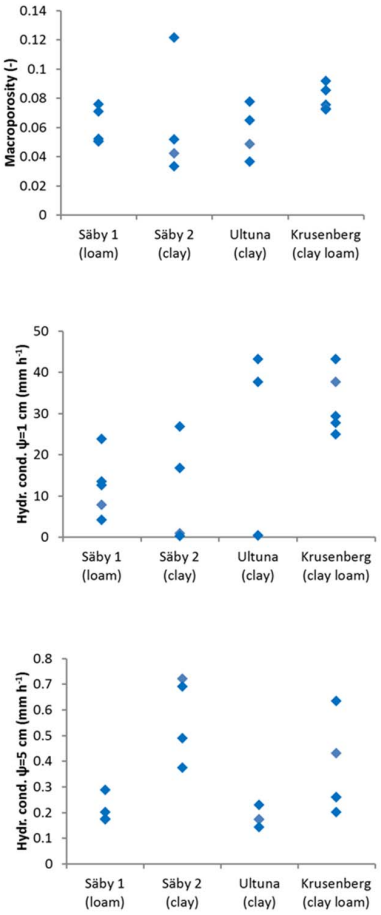

Figure 4. Macroporosities and near-saturated hydraulic conductivities for the four soils.

HESSD
11, 9551–9588, 2014

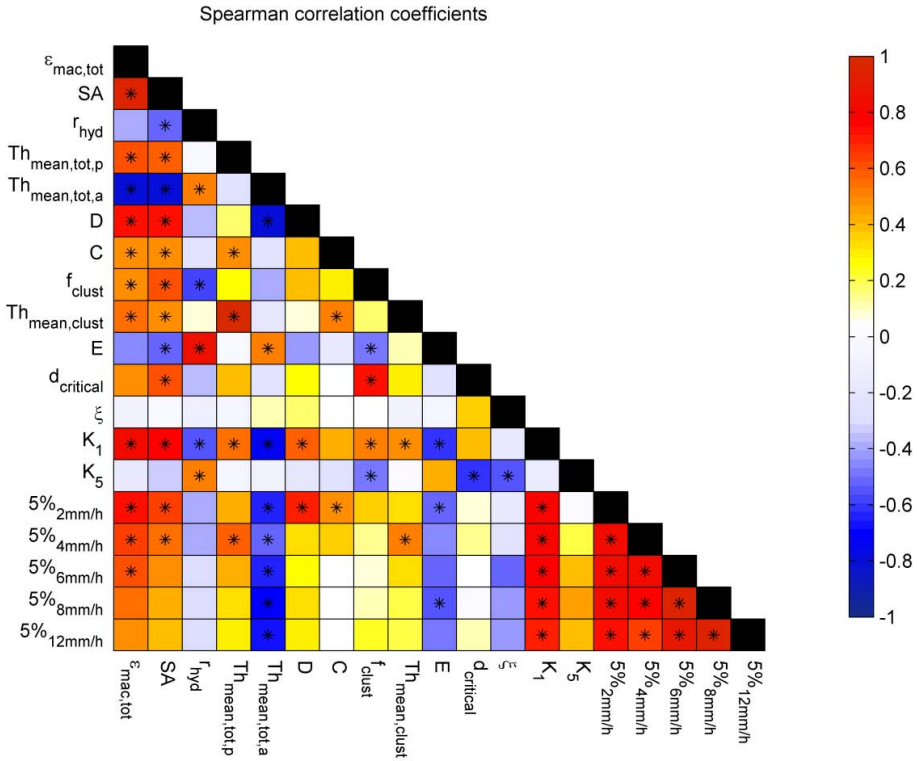

Figure 5. Spearman (rank) correlation coefficient between pore system characteristics, state variables and measures of preferential transport where $\varepsilon_{mac,tot}$, total macroporosity; SA, specific macropore surface area; r_{hyd}, hydraulic radius; $Th_{mean,tot,p}$, mean thickness of macropores; $Th_{mean,tot,a}$, mean thickness of soil matrix; D, fractal dimension; C, global connectivity; f_{clust}, fraction of cluster volume of total macropore volume; $Th_{mean,clust,p}$, mean thickness of macropores for cluster; E, Euler number; $d_{critical}$, critical pore diameter; ξ, tortuosity; K_1 and K_5, hydraulic conductivities at 1 and 5 cm tensions, respectively; $5\%_{X\,mm\,h^{-1}}$, 5 % arrival times at flow rates X mm h^{-1}. Stars indicate significant correlations ($p = 0.05$).

HESSD
11, 9551–9588, 2014

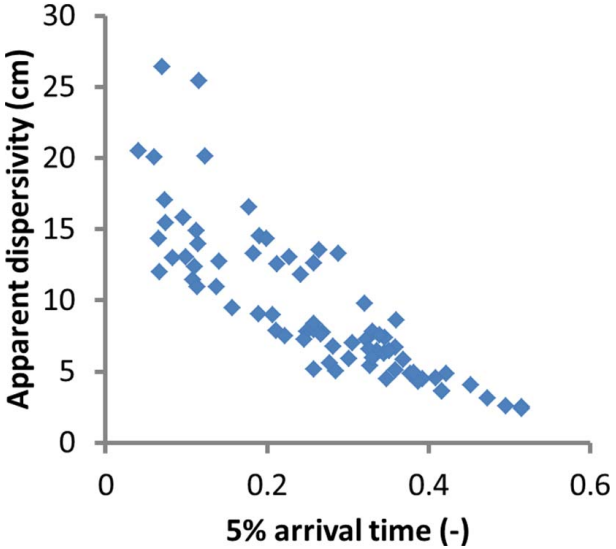

Figure 6. Correlations between measures of preferential transport.

HESSD
11, 9551–9588, 2014

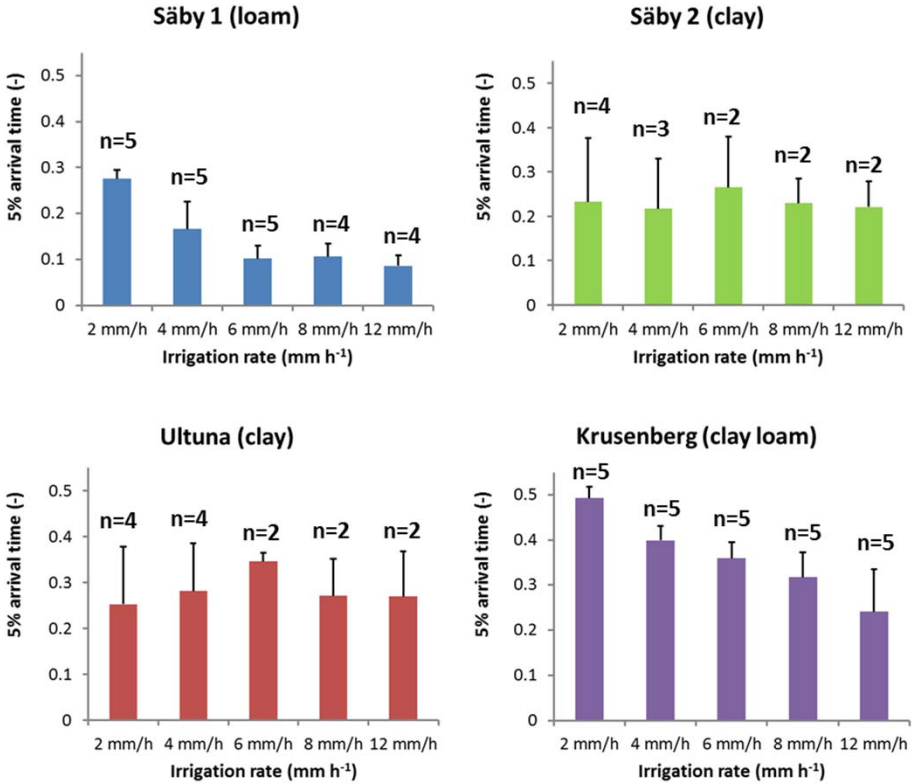

Figure 7. Mean 5 % arrival times for the four soils. The number of breakthrough curves, *n*, was smaller at higher irrigation rates due to ponding. Error bars indicate 1 standard deviation.

HESSD
11, 9551–9588, 2014

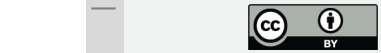

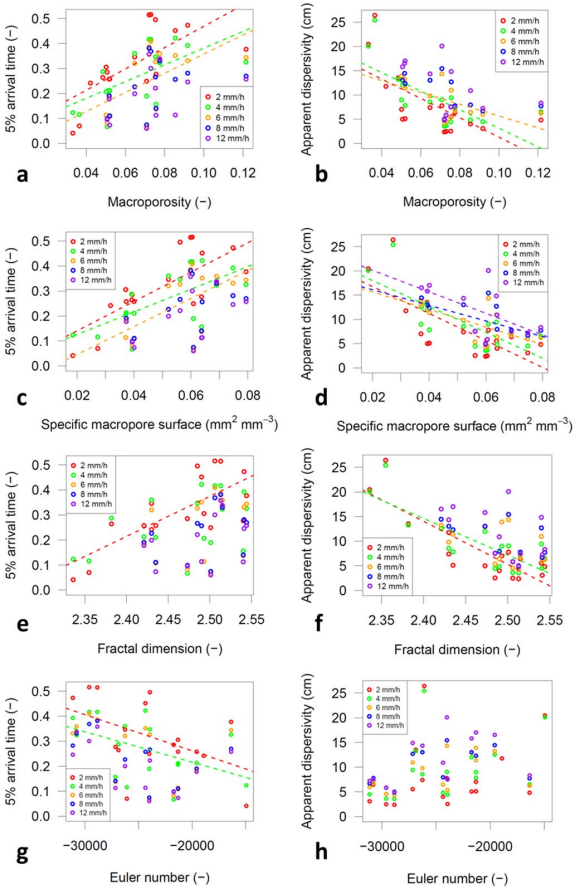

Figure 8. Relationship between macropore characteristics and measures of preferential transport for the four soils. Linear regression lines (dashed) were drawn if the slope was significantly (p = 0.05) different from zero.

HESSD
11, 9551–9588, 2014

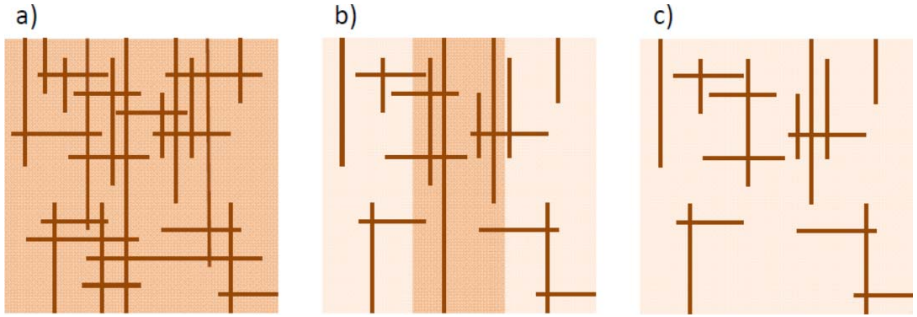

Figure 9. Schematic illustration of the relationship between local connectivity of the pore network, macroscopic (Darcy-scale) hydraulic conductivity and preferential transport **(a)** this represents a well-connected macropore network (a single pore cluster) with a uniformly high macroscopic hydraulic conductivity denoted by dark shading. The degree of preferential transport is consequently low **(b)** this network was created from the a-network by removing some pores to create seven isolated pore clusters. It represents a macropore network which is poorly connected locally, but which exhibits a high degree of preferential transport because one of the pore clusters is still continuous through the sample. At the Darcy scale, this is reflected in a continuous high conductivity pathway through the sample (dark shading) surrounded by low conductivity matrix (light shading) **(c)** this shows that removing one more pore results in a breakdown of sample-scale continuity, which will limit preferential transport. Macroscopic hydraulic conductivity is now uniformly low.

HESSD
11, 9551–9588, 2014

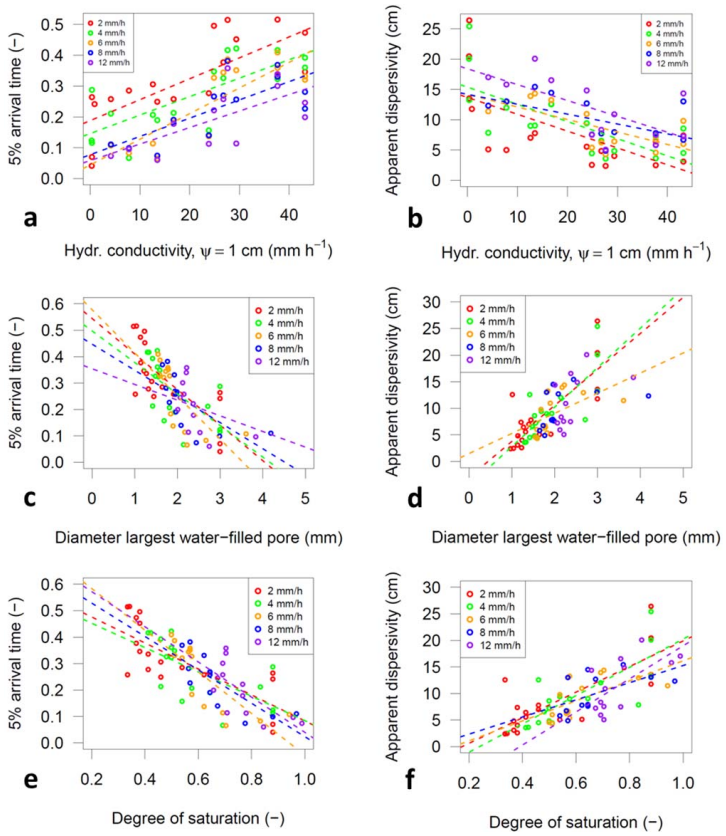

Figure 10. Relationship between hydraulic conductivity at ψ = 1 cm, the diameter of the largest water-filled pore, the degree of saturation and measures of preferential transport for the four soils. Linear regression lines (dashed) were drawn if the slope was significantly (p = 0.05) different from zero.

HESSD
11, 9551–9588, 2014